Solar Energy 262 (2023) 111748

Contents lists available at ScienceDirect

Solar Energy

journal homepage: www.elsevier.com/locate/solener

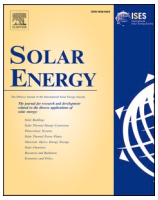

Integration of a lithium-ion battery in a micro-photovoltaic system: Passive versus active coupling architectures

René Behmann, Jack Phan, Artur Root, Michael Schmidt, Wolfgang G. Bessler [*,1]

Institute of Sustainable Energy Systems (INES), Offenburg University of Applied Sciences, Badstrasse 24, 77652 Offenburg, Germany

ARTICLE INFO

Keywords:
Micro photovoltaic (micro-PV)
Balcony solar
Battery
Passive hybridization
Active hybridization
Self-consumption

ABSTRACT

A balcony photovoltaic (PV) system, also known as a micro-PV system, is a small PV system consisting of one or two solar modules with an output of 100–600 Wp and a corresponding inverter that uses standard plugs to feed the renewable energy into the house grid. In the present study we demonstrate the integration of a commercial lithium-ion battery into a commercial micro-PV system. We firstly show simulations over one year with one second time resolution which we use to assess the influence of battery and PV size on self-consumption, self-sufficiency and the annual cost savings. We then develop and operate experimental setups using two different architectures for integrating the battery into the micro-PV system. In the passive hybrid architecture, the battery is in parallel electrical connection to the PV module. In the active hybrid architecture, an additional DC-DC converter is used. Both architectures include measures to avoid maximum power point tracking of the battery by the module inverter. Resulting PV/battery/inverter systems with 300 Wp PV and 555 Wh battery were tested in continuous operation over three days under real solar irradiance conditions. Both architectures were able to maintain stable operation and demonstrate the shift of PV energy from the day into the night. System efficiencies were observed comparable to a reference system without battery. This study therefore demonstrates the feasibility of both active and passive coupling architectures.

1. Introduction

Photovoltaic (PV) technology is an excellent means to generate renewable, climate-neutral electricity. Due the intermittent nature of PV power generation, electricity storage is of high importance for both enabling high self-sufficiency and maintaining a stable electricity grid [1,2]. This is also reflected in the sales figures for home storage systems, which have been rising steadily for years [3,4]. Home storage systems typically comprise of a 5–15 kWh scale battery coupled to 5–15 kWp rooftop PV system. Different electrical architectures are used for coupling battery and photovoltaics. Alternating current (AC) architectures consist of a direct current/alternating current (DC/AC) conversion between PV and house grid, and additional DC/AC conversion between battery and house grid, which provides flexibility in terms of modularity and extensibility. DC architectures consist of DC/DC conversion between PV and battery with subsequent DC/AC conversion to house grid, which provides higher conversion efficiency [5]. As PV and battery represent a hybrid power generation system, we have used the term *active hybridization* for these standard architectures [6,7].

In addition to rooftop PV systems, there is also a large potential for so-called micro-PV systems. These systems consist of only one or two PV panels with an output of 100–600 Wp. They come with a small outdoor DC/AC inverter (also referred to as microinverter due to the comparatively low power) that features maximum power point (MPP) tracking (MPPT) [8]. The inverter is coupled to the house grid via a regular plug. Micro-PV systems can be easily installed on balconies, terraces, or façades, and are therefore also referred to as balcony PV systems [9]. They are particularly interesting for tenants without own house, who can participate in the energy transition in this way through simple installation. If low prizes can be realized, micro-PV systems have the potential for mass introduction and significant contribution to renewable energy supply.

Fig. 1 summarizes the approach of the present study. So far, commercially-available grid-coupled micro-PV systems (Fig. 1a), different to larger rooftop PV systems, do not feature the possibility to integrate battery storage. At the same time, medium-sized lithium-ion batteries, for example from electric bicycles (e-bikes), are easily accessible and today available in many households. Therefore, the novelty of

* Corresponding author.
E-mail address: wolfgang.bessler@hs-offenburg.de (W.G. Bessler).
[1] Member of the International Solar Energy Society (ISES).

https://doi.org/10.1016/j.solener.2023.05.025
Received 19 December 2022; Received in revised form 15 April 2023; Accepted 17 May 2023

this work is the integration of a commercial lithium-ion battery (Fig. 1b) into a commercial micro-PV system. As in regular home-storage systems, this allows to increase PV self-consumption and the degree of self-sufficiency by shifting energy from day into the night. In order to keep the system cost low, the coupling should use as little additional components as possible. Additionally, the two subsystems (micro-PV system with module inverter and lithium-ion battery) should not require any modification. As will be discussed in this paper, this is particularly challenging as the MPP tracker of the module inverter does not "know" that it is connected to a battery, requiring passive or active measures to avoid MPP tracking of the battery. In order to fulfill these requirements, we have developed two different coupling architectures between PV module, battery and inverter. We refer to these two configurations as *passive hybridization* (Fig. 1c) and as *active hybridization* (Fig. 1d).

Passive hybridization, also referred to as "direct coupling" [10], means the parallel electrical connection of PV module and battery without any inverters or charge controllers in between. The principle reaches back to 1968 when first patents were filed [11,12]. It is based on matching the PV and the battery respective current and voltage behaviors. During battery charge, the system voltage increases and drives the PV towards zero current when the battery is fully charged. During discharge, a diode protects the PV from too low voltage levels. Due to the self-regulation of the system, no active battery management system (BMS) is required to protect the battery against overcharging. Even more, the simple architecture makes the system more robust and less expensive compared to standard systems. The main disadvantage of the system is the reduced efficiency, since the PV is no longer operating continuously at the MPP [7]. Astakhov et al. [10], Joos et al. [6], Kakimoto et al. [13] and Ayeng'o et al. [14] have used modeling and simulation to assess the coupling efficiency as a function of various design parameters, for example, the number of serially-connected single battery cells (hence, battery voltage) or the temperature. Experimental demonstrations were carried out using single battery cells, including the work by Agbo et al. (1.9 V lithium-ion Swagelok cell) [15], Leible et al. (2.3 V lithium-ion cell) [7], Kin et al. (3.7 V lithium-ion cell) [16] and Chibuko et al. (3.7 V lithium-ion cell) [17]; and full batteries, including work by Gibson et al. (33 to 53 V lithium-ion batteries) [18], Kakimoto et al. (18 V lithium-ion battery) [13], and Ayeng'o et al. (24 V lead-acid battery) [14]. The recent work of Chibuko et al. [17] and Shcherbachenko et al. [19] demonstrated that a careful design of battery and PV voltage levels can provide coupling efficiencies comparable to MPP-tracked setups. It is interesting to note that the challenge of matching PV and battery properties are also part of the attempt to sandwich storage elements directly into a PV module, as has recently been reviewed by Vega-Garita et al. [20].

In active hybridization, power electronics and a controller are connected between the battery and PV systems to actively control voltages and currents and regulate the interaction between the components. Here, one side of a controller is placed in the parallel connection between PV modules and inverter. The battery is connected on the other side of the controller. In both our investigated configurations, passive and active hybridization, we use the regular micro-PV inverter for feeding the PV and/or battery power into the house grid. In order to evaluate the two configurations in terms of efficiency, a reference system without battery was also investigated.

Modeling and simulation have proven powerful tools for assessing the performance of PV systems and PV-battery systems [21–23]. A review of professional simulation software was recently published by Milosavljevic et al. [24]. In the present work, in addition to the experimental studies, we have carried out system simulations of micro-PV/battery systems. Based on real weather data and high-resolution synthetic load profiles, the simulation is used to assess the performance of typical balcony installations over one year of operation as a function of PV peak power and battery energy. To this goal, we apply an in-house code used previously for assessing the performance and lifetime of PV-battery systems [6,25]. The simulation results were also used for initial system prototyping.

The paper is organized as follows. Section 2 describes the simulation approach and Section 3 presents the experimental setup of the PV-battery systems. Section 4 shows and discusses the results. Finally, Section 5 concludes the article.

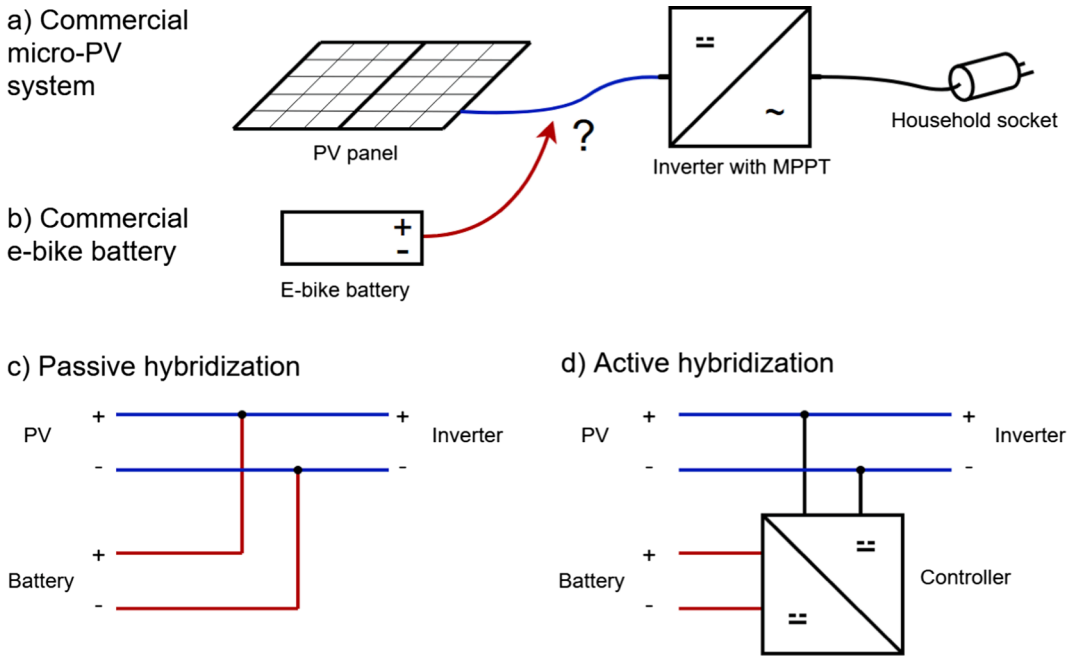

Fig. 1. The present study demonstrates the integration of a commercial lithium-ion battery for e-bikes (b) into a commercial micro-PV system (a) that features an inverter with maximum power point tracker (MPPT). To this goal, two different coupling architectures are developed, called here passive hybridization (c) and active hybridization (d).

2. Simulation methodology

2.1. Modeling and simulation approach

In order to obtain a better understanding of the properties and performance of battery-coupled micro-PV systems, a modeling and simulation study was carried out. The simulations were used to dimension the different components of the system and to compare different energy management strategies in order to obtain and assess important parameters of the system, in particular, the PV self-consumption, the degree of self-sufficiency and the annual cost savings.

To this goal, we have used an in-house model implemented in MATLAB/SIMULINK (R2021b). There are two reasons for using the in-house model, as compared to commercial simulation codes [24]. Firstly, it allows flexible parametric studies and visualization, as will be shown below. Secondly, we have used the same model before in the context of simulating passive hybrid systems [6] by coupling it to a system model, and in the context of battery lifetime prediction [25] by coupling it to a physics-based battery aging model. This kind of model coupling is not possible with commercial codes.

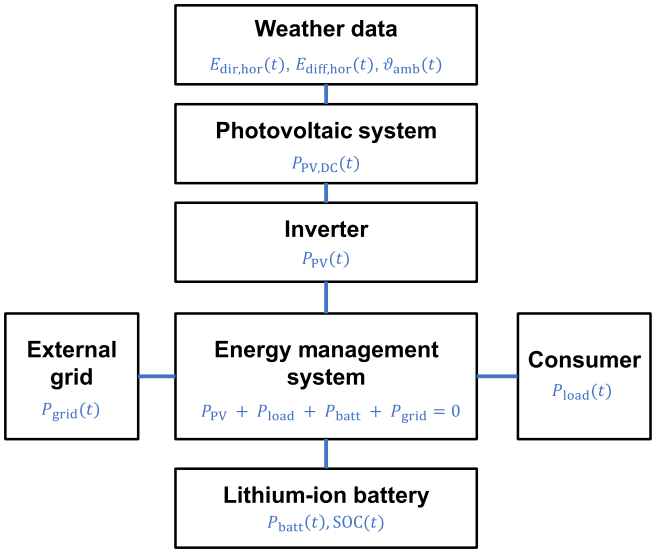

Fig. 2. Schematic representation of the system model including the dynamic states of the subsystems.

The modeling approach is shown in Fig. 2. The full set of model equations is given in Table 1, and all model parameters are given in Table 2. As the model was published before [6,25], only a brief summary is given here. Historic weather data (direct and diffuse irradiation and temperature) for the location of Offenburg University of Applied Sciences, Offenburg, Germany [26] are used as system input. For the present simulation, a data set for the complete year 2014 with a resolution of 1 min was used. The weather data are converted to the total irradiation (consisting of direct, diffuse, and reflected irradiation) normal to the PV module taking standard equations from Quaschning [5] and Klucher [27] (Table 1, Eqs. 1–14). The PV module is assumed to continuously operate at MPP. Current and voltage at MPP are calculated using expressions from Quaschning [5] (Table 1, Eqs. 15–18). Other effects such as shading and module aging are not considered in this simulation. The AC-side output power of the inverter is modeled by means of the PV power and an efficiency factor (Table 1, Eq. 19). The efficiency factor is assumed to be constant at this point and is taken from the data sheet of a commercial inverter [28]. The load is assumed to represent a single-family house with an annual demand of 3344 kWh, using a synthetic load profile with 1 min time resolution [29]. We furthermore assume a grid-connected system, which means that electrical power can be consumed from or fed into the external power grid. The battery is modeled using a single energy balance equation, including a constant efficiency factor (Table 1, Eqs. (20) and (21)). To keep the battery operation within the voltage and current limits, a simple BMS was implemented, limiting the charging or discharging power and state of charge (SOC) range. The power fluxes between the system components (PV, battery, load, grid) is controlled by a simple energy management system (EMS). It describes the respective power flows between the subsystems such that the power balance (Table 1, Eq. (22)) is always satisfied. Here, the electric power P is defined as positive when the power enters the EMS and negative when the power leaves the EMS. The battery power P_{batt} is the parameter controlled by the EMS, while P_{load} and P_{PV} are given by the respective subsystems. P_{grid} is obtained from the power balance. The EMS is decision based, always giving priority to battery charge/discharge over grid charge/discharge.

Table 1
Model equations. See Table 2 for symbol definitions.

System component	*Model equation*	
Weather data		
Global irradiance on inclined module	$E_{gen} = E_{dir,gen} + E_{diff,gen} + E_{refl,gen}$	(1)
Direct irradiance on the inclined module	$E_{dir,gen} = E_{dir,hor} \cdot \frac{\cos\theta_{gen}}{\sin\gamma_S}$	(2)
Diffuse irradiance on the inclined module	$E_{diff,gen} = E_{diff,hor} \cdot \frac{1}{2} \cdot (1 + \cos\gamma_E) \cdot \left(1 + F_E \cdot \left(\sin\frac{\gamma_E}{2}\right)^3\right) \cdot \left(1 + F_E \cdot (\sin\theta_{gen})^2 \cdot (\sin\gamma_S)^3\right)$	(3)
Reflected irradiance on the inclined module	$E_{refl,gen} = (E_{dir,hor} + E_{diff,hor}) \cdot A \cdot \frac{1}{2} \cdot (1 - \cos\gamma_E)$	(4)
Clearness index	$F_E = 1 - \left(\frac{E_{diff,hor}}{E_{dir,hor} + E_{diff,hor}}\right)^2$	(5)
Angle of incidence	$\theta_{gen} = \arccos(-\cos\gamma_S \cdot \sin\gamma_E \cdot \cos(\alpha_S - \alpha_E) + \sin\gamma_S \cdot \cos\gamma_E)$	(6)
Sun elevation angle	$\gamma_S = \arcsin(\cos\omega \cdot \cos\varphi \cdot \cos\delta + \sin\varphi \cdot \sin\delta)$	(7)
Sun azimuth angle	$\alpha_S = \begin{cases} 180^\circ - \arccos\left(\frac{\sin\gamma_S \cdot \sin\varphi - \sin\delta}{\cos\gamma_S \cdot \cos\varphi}\right) & \text{for } WOZ \le 12:00\ h \\ 180^\circ + \arccos\left(\frac{\sin\gamma_S \cdot \sin\varphi - \sin\delta}{\cos\gamma_S \cdot \cos\varphi}\right) & \text{for } WOZ > 12:00\ h \end{cases}$	(8)
Local hours angle	$\omega = (12:00\ \text{h} - \text{WOZ}) \cdot 15^\circ/\text{h}$	(9)
Declination of sun	$\delta = \{0.3948 - 23.2559 \cdot \cos(J' + 9.1^\circ) - 0.3915 \cdot \cos(2 \cdot J' + 5.4^\circ) - 0.3915 \cdot \cos(3 \cdot J' + 26^\circ)\}^\circ$	(10)
Equation of time	$Zgl = \{0.0066 + 7.3525 \cdot \cos(J' + 85.9^\circ) + 9.9359 \cdot \cos(2 \cdot J' + 108.9^\circ) + 0.3387 \cdot \cos(3 \cdot J' + 105.2^\circ)\}\ \text{min}$	(11)
Day of year	$J' = 360^\circ \cdot \frac{d}{\text{number days per year}}$	(12)
True local time	$\text{WOZ} = \text{MOZ} + \text{Zgl}$	(13)

(*continued on next page*)

Table 1 (*continued*)

System component	*Model equation*	
Local mean time	$\mathrm{MOZ} = (t_{\mathrm{CET}} - 60\ \mathrm{min}) + 4 \cdot \lambda \cdot \frac{\mathrm{min}}{^\circ}$	(14)
PV module		
Power output	$P_{\mathrm{PV,DC}} = I_{\mathrm{MPP}} \cdot V_{\mathrm{MPP}}$	(15)
Current at MPP	$I_{\mathrm{MPP}} = I_{\mathrm{MPP,STC}} \cdot \frac{E_{\mathrm{gen}}}{E_{\mathrm{STC}}} \cdot (1 + \alpha_{\mathrm{I}} \cdot (\vartheta_{\mathrm{mod}} - \vartheta_{\mathrm{STC}}))$	(16)
Voltage at MPP	$V_{\mathrm{MPP}} = V_{\mathrm{MPP,STC}} \cdot \frac{\ln(E_{\mathrm{gen}})}{\ln(E_{\mathrm{STC}})} \cdot (1 + \alpha_{\mathrm{V}} \cdot (\vartheta_{\mathrm{mod}} - \vartheta_{\mathrm{STC}}))$	(17)
Module temperature	$\vartheta_{\mathrm{mod}} = \vartheta_{\mathrm{amb}} + c \cdot \frac{E_{\mathrm{gen}}}{E_{\mathrm{STC}}}$	(18)
Inverter		
AC Output power	$P_{\mathrm{PV,AC}} = P_{\mathrm{PV,DC}} \cdot \eta_{\mathrm{inv}}$	(19)
Lithium-ion battery		
Energy increase	$\frac{\mathrm{d}E_{\mathrm{batt}}}{\mathrm{d}t} = -P_{\mathrm{batt}} \cdot \begin{cases} 1/\eta_{\mathrm{batt}} & (\mathrm{for}\, P_{\mathrm{batt}} > 0,\ \mathrm{discharge}) \\ \eta_{\mathrm{batt}} & (\mathrm{for}\, P_{\mathrm{batt}} < 0,\ \mathrm{charge}) \end{cases}$	(20)
State of charge	$\mathrm{SOC} = \frac{E}{E_{\mathrm{N}}}$	(21)
Energy management system		
Power balance	$P_{\mathrm{PV}}(t) + P_{\mathrm{load}}(t) + P_{\mathrm{batt}}(t) + P_{\mathrm{grid}}(t) = 0$	(22)

2.2. Energy management strategies

In the present study, two different energy management strategies were investigated, a self-consumption optimization strategy (Scenario I) and a base load coverage strategy (Scenario II). Scenario I describes a system that knows P_{load} of the household (e.g., due to measurement of the power at the grid connection point) and tries to cover it via the PV generation or via the storage. The simpler Scenario II does not require knowledge of the load; instead, an assumed fixed or dynamically varying P_{load} is fed into the household. We study either constant base loads of 50 W or 100 W, or a dynamically-varying base load following the VDEW H0 load profile, which has 15 min resolution [30] and which we scaled to the annual PV production. Remember that, for either scenario, the EMS attempts to satisfy P_{load} firstly with the PV and secondly with the battery.

In order to assess the performance of the system, four key performance indicators were quantified. Annual self-consumption (SC) is the ratio between self-consumed and produced PV energy, which can be expressed as

$$\mathrm{SC} = \left(1 - \frac{\int_{P_{\mathrm{grid}<0}} - P_{\mathrm{grid}}\ \mathrm{d}t}{\int P_{\mathrm{PV}}\ \mathrm{d}t}\right) \cdot\ 100\ \%, \tag{23}$$

where, the integral in the numerator denotes the power that is fed by the system into the grid. The integrals in this and the following equations run over the entire simulated year. Annual self-sufficiency (SS) is the fraction of the load demand that is covered locally (through PV or battery storage, where battery and inverter losses are included). It can be expressed as

$$\mathrm{SS} = \left(1 - \frac{\int_{P_{\mathrm{grid}>0}} P_{\mathrm{grid}}\ \mathrm{d}t}{\int -P_{\mathrm{load}}\ \mathrm{d}t}\right) \cdot\ 100\ \%, \tag{24}$$

where, the integral in the numerator denotes the power consumed by the system from the grid. Furthermore, in order to assess economic viability, the annual savings (AS) from the system were quantified as

$$\mathrm{AS} = C_{\mathrm{grid}} \cdot \frac{\mathrm{SS}}{100\ \%} \cdot \int -P_{\mathrm{load}}\ \mathrm{d}t \tag{25}$$

where, C_{grid} is the energy-specific end-consumer electricity price and the integral represents the annual electricity consumption. For C_{grid}, we use the average end-consumer prize in Germany as of April 2022, of 0.357 €/kWh [31]. Finally, the amortization time (AT) was quantified as

$$\mathrm{AT} = \frac{C_{\mathrm{batt}} \cdot E_{\mathrm{batt}} + C_{\mathrm{PV}} \cdot P_{\mathrm{PV}}}{\mathrm{AS}} \tag{26}$$

where, C_{batt} is the energy-specific battery prize and C_{PV} is the power-specific PV module prize.

In order to quantify the values for C_{batt} and C_{PV}, we carried out an internet-based market research on systems available in/shippable to Germany as of April 2023. For the battery, this included 97 individual e-bike batteries from 14 manufacturers (Bafang, Bosch, Continental, E-Bike vision, Fit, Giant, Groove, Haibike, Impulse, Mahle, Panasonic, Shimano, TQ, Yamaha) with energy capacities between 200 Wh and 925 Wh (average: 524 Wh) at end-consumer prizes between 299 € and 1199 €. The average energy-specific battery prize was 1366 €/kWh. For the PV, this included 125 individual micro-PV systems from 11 manufacturers (Anker, BalkonKraftwerk, GreenAkku, GreenSolar, Kleines Kraftwerk, McSolar, Mein Solarwerk, Priwatt, Tinosolar, Venturama, Yuma) with module peak powers between 200 Wp and 4920 Wp (average: 959 Wp). The average power-specific PV module prize was 1019 €/Wp. In the latter number, the cost for the microinverter is included. Note that installation costs are not included in the present analysis because micro-PV systems are generally made for self-installation.

3. Experimental methodology

3.1. Approach

The investigated micro-PV/battery systems are based on two novel interconnection concepts, here referred to as passive and active hybridization, as described in more detail below. Both systems consist of three series-connected PV modules (BeON, ETFE flexible solar panel) of 100 Wp each (open-circuit voltage $V_{\mathrm{OC}} = 14.8$ V, short circuit current $I_{\mathrm{SC}} = 9.07$ A), a 36 V electric bicycle LIB (LionTec, Season) with a nominal energy of 555 Wh and a nominal capacity of 15.5 Ah, and a 250 W inverter (BeON 1) with MPP tracker. To evaluate the two new systems in terms of their respective efficiencies, a reference system without a battery was also investigated. The system architectures are shown in Fig. 3 and will be discussed further below.

All experiments were carried out on a rooftop laboratory under open air. DC measurements were made for all systems using two portable data

Table 2
Model parameters.

Parameter	*Value*	*Reference*
Weather data		
Direct irradiation $E_{dir,hor}$, diffuse irradiation $E_{diff,hor}$, temperature ϑ_{amb}	Historic data of year 2014	[26]
Inclination angle of module γ_E	31.7°	*
Orientation angle of module α_E	13.3°	*
Geographical latitude of module φ	48.458°	*
Geographical longitude of module λ	7.943°	*
Albedo factor A	0.2	[5]
PV module		
Peak power at STC	Varies	This study
Radiation at STC E_{STC}	1000 W·m^{-2}	[32]
Temperature at STC ϑ_{STC}	25 °C	[32]
Open-circuit voltage at STC $V_{OC,STC}$	37.1 V	[32]
Short-circuit current at STC $I_{SC,STC}$	8.5 A	[32]
Voltage at MPP and STC $V_{MPP,STC}$	29.9 V	[32]
Current at MPP and STC $I_{MPP,STC}$	8.0 A	[32]
Current temperature coefficient α_I	−0.32 %·K^{-1}	[32]
Voltage temperature coefficient α_V	0.032 %·K^{-1}	[32]
PV temperature coefficient c	28 °C	[5]
Inverter		
Efficiency η_{inv}	0.85	[28]
Lithium-ion battery		
Nominal energy E_N	Varies	This study
Efficiency η_{batt}	0.95	Assumed
Economic parameters		
Electricity cost C_{grid}	0.357 €/kWh	See text
Battery cost C_{batt}	1366 €/kWh	See text
PV module cost C_{PV}	1019 €/kWp	See text

* PV system at Offenburg University of Applied Sciences, Offenburg, Germany.

loggers (Graphtec, GL240) with ten input channels each. The voltage measurement range of the channels is between 20 mV and 50 V and was selected depending on the measurement point. The accuracy is ± 0.1 %. Shunt resistors with a voltage drop of 30 mV at a current of 50 A were used to measure the current at different positions. For active hybridization, the controller current and battery current are measured using onboard shunt resistors with a voltage drop of 30 mV at a current of 15 A. AC characteristics were recorded inductively using a portable data logger (Chauvin Arnoux, PEL103). Weather data were obtained from measurements at the weather station of the Offenburg University of Applied Sciences [26]. The three systems (passive hybrid, active hybrid, reference) were tested on separate days with different meteorological conditions. For both AC and DC measurements, data was recorded in one-second increments. Weather data were recorded in ten-minute increments. MATLAB (R2021b) was used to analyze the extensive data sets.

Battery SOC was determined as

$$\mathrm{SOC}(t) = \frac{Q(t)}{C} = \frac{\int_0^t -I(t)\mathrm{d}t}{C} \tag{27}$$

where, I is the measured battery current and Q the charge content obtained by time-integrating the current. The initial SOC of the battery (30 % in the passive hybridization experiment, 98.5 % in the active hybridization experiment) was determined by comparing the battery rest voltage to the open-circuit voltage curve recorded before using a battery cycler (Biologic FlexP 0160).

3.2. Reference system

The reference system is shown in Fig. 3a). It consists of the PV modules connected to the inverter. For the subsequent discussion of the hybrid systems, it is important to note that the inverter features an MPP tracker: The control algorithm probes the current–voltage characteristics of the PV modules and dynamically follows the MPP during the complete operation time.

3.3. Passive hybrid system

The passive hybrid system is shown in Fig. 3b). The main components are the PV modules, the LIB, and the inverter, all connected in parallel. In addition to these components, the passive hybrid system consists of a diode (PanJit Schottky Diode, SBT1545LSS), a resistor (5 Ω) and several switches for isolation purposes. The diode prevents the PV modules from discharging the battery during the night when the PV voltage is lower than the battery voltage. Diodes are typically being used in passive hybrid architectures [6,7,11,12,18].

The resistor connected in series with the inverter ensures that the corresponding current flow is throttled, for the following reason. LIB have a restricted operation voltage range (typical cut-off voltages around 3.0 V to 4.2 V per cell), outside of which the battery is subject to fast aging [33] or even thermal runaway [34,35]. On the contrast, PV cells are operated in voltage ranges between 0 V and 0.7 V per cell. As a result of the different voltage ranges, a PV cell has an MPP, while a LIB does not. In the present setup, the LIB is directly connected to an inverter with MPP tracker. Without further protection, the MPP tracker would drive the LIB to voltages below the cut-off voltage, resulting in very high currents and severe damage to the battery. This is prevented by the serial resistor. However, while needed to protect the battery, the resistor increases losses in the system, as it also reduces the current generated by the PV.

At this point, it becomes clear that the choice of the resistor is crucial for the operating characteristics of the system. Assuming an idealized battery with constant voltage V^0_{batt}, internal resistance R_{batt}, and a protective series resistor with resistance R_s, the combined $V(I)$ characteristics are given as

$$V_{batt\&res}(I) = V_{batt}(I) - V_{res}(I) = V^0_{batt} - R_{batt}\cdot I - R_s\cdot I \tag{28}$$

The power is given as $P = V\cdot I$, and the MPP given through the condition $\mathrm{d}P/\mathrm{d}I = 0$. From these equations, it is straightforward to derive the MPP properties as

$$I_{MPP} = \frac{V^0}{2(R_{batt} + R_s)} \tag{29}$$

$$V_{MPP,batt\&res} = \frac{1}{2}V^0 \tag{30}$$

$$V_{MPP,batt} = V^0\left(1 - \frac{R_{batt}}{2(R_{batt} + R_s)}\right) \tag{31}$$

Assuming typical values of $V^0_{batt} = 36$ V and $R_{batt} = 0.1$ Ω (representing the battery used here) results for a system without series resistor ($R_s = 0$ Ω) in an MPP voltage of $V_{MPP,batt} = 18$ V and $I_{MPP} = 180$ A, which is far outside the cut-off voltage of 30 V and maximum current of 15 A (1C rate of the LIB used here). Adding a series resistor of $R_s = 5$ Ω (this work) results in $V_{MPP,batt} = 35.6$ V and $I_{MPP} = 3.5$ A (0.23C rate), which is well within the operation characteristics.

3.4. Active hybrid system

3.4.1. Overview

The active hybrid system is shown in Fig. 3c). It differs from the passive hybrid by the introduction of an additional controller, based on a

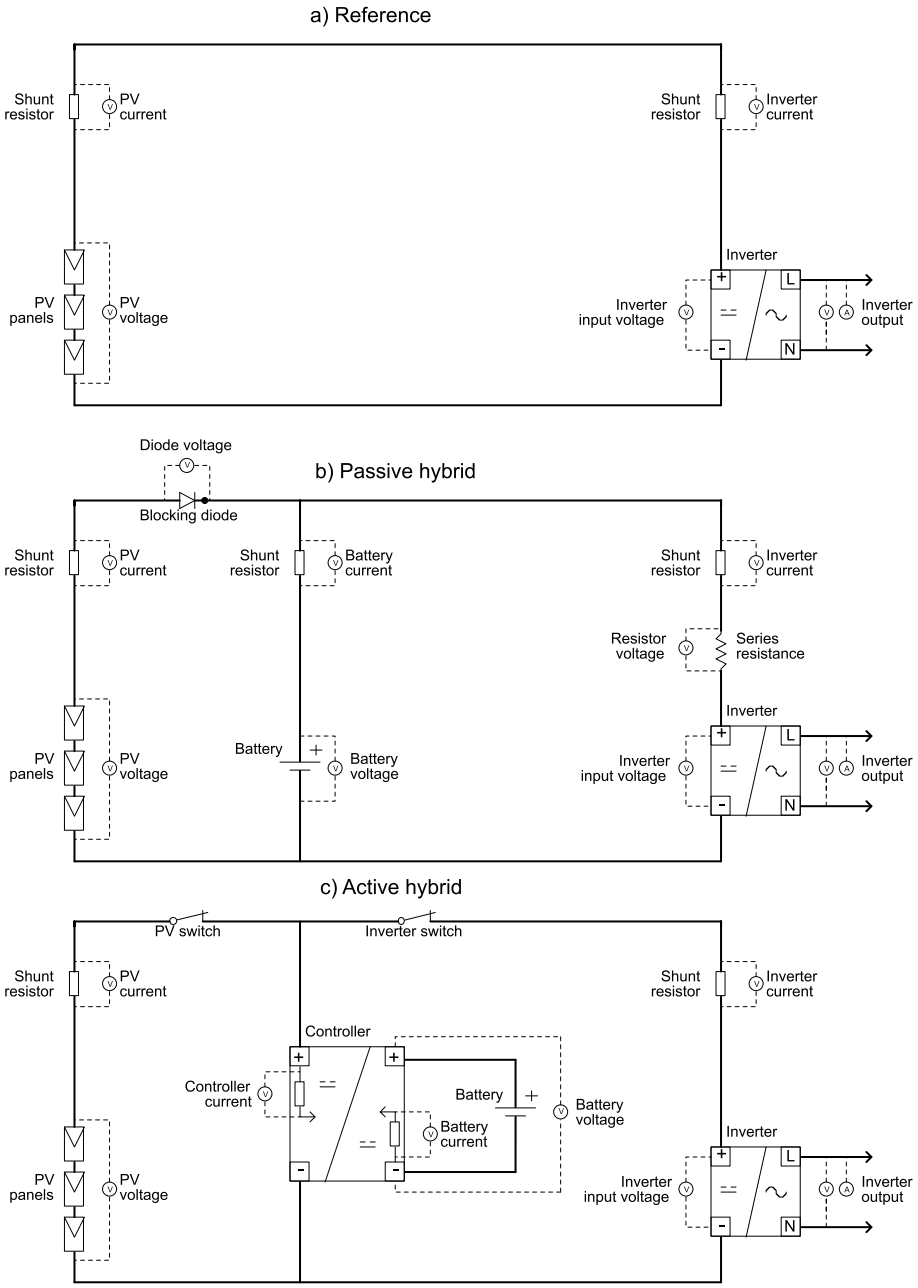

Fig. 3. System architectures and monitoring concepts of a) the reference system, b) the passive hybrid system, c) and the active hybrid system.

DC-DC converter, between the battery and the parallel connection between PV modules and inverter. No blocking diode is used, as the controller uses a built-in electromechanical relay that disconnects the PV modules from the system during the supply phase (battery discharge). There is no series resistor as the controller regulates the allowable power to the inverter. The controller is based on a bidirectional buck/boost converter that allows current to flow to charge the battery in one direction and discharge the battery in the other direction. The controller is controlled by a 16-bit microcontroller (Texas Instruments MSP430F5529) and has integrated measurement and control circuits that allow fully automatic operation. There is no communication between the controller and the micro-PV inverter or other external devices. A configurable real-time clock controls when each mode of operation starts. For the experiment presented here, the controller is set to charge the battery starting at 6 a.m. each day and discharge the battery (to power the micro-PV inverter) at 10 p.m. each day. The controller enters an energy-saving sleep mode if the battery is fully charged before the supply phase begins, and likewise if the battery is fully discharged before the charging phase begins.

3.4.2. *Battery charge*

In the charge mode of the controller, both the PV switch and the inverter switch in Fig. 3c are closed. Accordingly, all components, i.e. PV modules, controller and inverter are then operated simultaneously and in parallel. The PV current is divided into a charging current for the battery and a current for the inverter, which is then fed into the house grid. The way in which the current is divided up satisfies the known rules of parallel connection depending on the resistance of controller and inverter. To achieve faster charging of the battery, the inverter switch could also be opened and the inverter disconnected from the system. However, this option was not experimentally investigated in the present work.

In the following, the charging method of the controller is described first without considering the interaction with the inverter. A

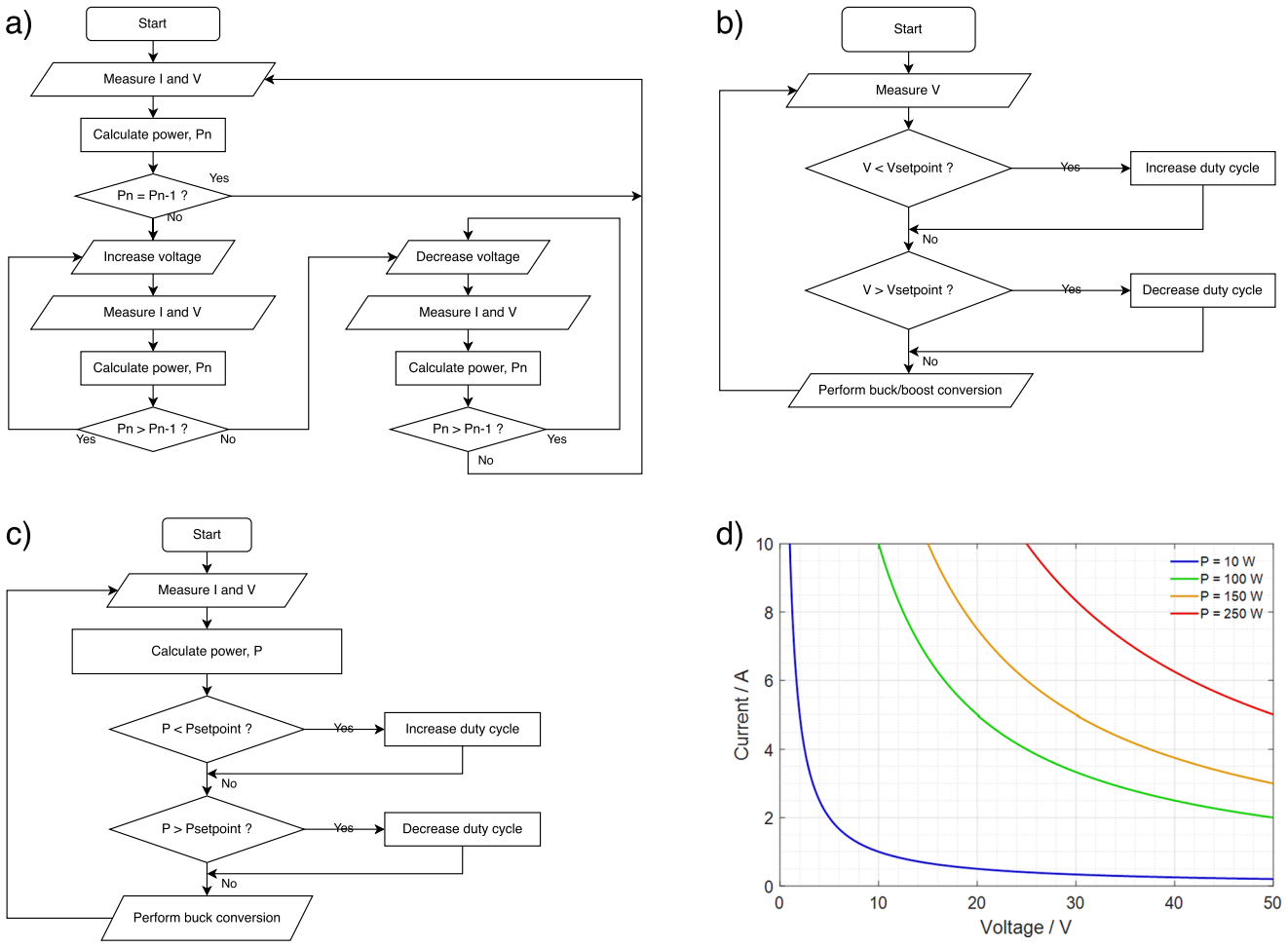

Fig. 4. Flow charts for the battery controller. a) Battery charge with MPPT, b) battery charge under constant voltage, c) battery discharge under constant power, d) and power regulation *I-V* characteristics.

combination of step-down conversion (buck) and step-up conversion (boost) is used for charging. The controller uses a customized MPPT algorithm to charge the battery for battery voltages up to the end-of-charge voltage. MPP charging replaces the constant-current phase of common constant-current constant-voltage (CCCV) charging protocols for LIB. It ensures efficient use of solar resources at any given time, based on current meteorological and physical conditions. When the end-of-charge voltage is reached, the controller continues to charge the battery at constant voltage (CV). When the charging current drops below 180 mA (C/85 rate), the CV phase ends, and the controller goes into sleep mode.

Our MPP charging algorithm is based on the well-known "perturb and observe" algorithm [36]. The program flow diagram is shown in Fig. 4a). The controller first reads current and voltage on the PV side. Then the operating power is calculated and compared with the previous value. If the value is the same, the reading and comparison process is repeated until a change is detected. Then the output voltage of the controller is arbitrarily increased ("perturb"), the output current and voltage are read again, and the power is calculated again. The power is then compared to the previous value ("observe"). If an increase in voltage has resulted in an increase in power, the voltage is increased again, and the process is repeated until a negative change in power is observed. A negative power change will cause the controller to repeat the "perturb" and "observe" steps, but instead of increasing the output voltage, it will decrease it. The entire process is repeated until negative power change is observed again. Fig. 4b) shows the program flow chart for CV charging. When entering the CV phase, the battery voltage is read. This voltage is compared to a predefined voltage set point. If the voltage is less than the setpoint, the duty cycle of the step-down or step-up conversion is increased, which increases the battery voltage. On the other hand, if the voltage is greater than the setpoint, the duty cycle of the step-down or step-up conversion is decreased, causing the voltage on the battery side to decrease. This process is repeated to maintain the desired voltage setpoint. The decision whether to perform a step-down or step-up conversion depends on the current PV voltage.

As mentioned at the beginning, controller and inverter were operated simultaneously and in parallel in the experiment presented in this work. Both components pursue the same goal, that is, to operate the respective connected components at MPP. However, as both two components are controlled separately, smooth interaction requires particular attention, in particular to avoid power oscillations or domination by one single component. To at least limit this possibility, both a minimum permissible and a maximum permissible charging current were defined for the controller. For this experiment, limits of 250 mA and 2.5 A (C/6 rate) were set, respectively. In this way, stable operation could be realized. Since the inverter MPP parameters or methods were not known and could not be changed, further theoretical investigation is out of scope of the present work.

3.4.3. *Battery discharge*

In the controller's discharge mode, current flows from the battery to the inverter. During this process, the PV modules are disconnected from the system via a built-in electromechanical relay (the PV switch in Fig. 3c). The MPPT of the inverter is designed to find the MPP voltage for

a typical *I-V* curve of solar modules and maintain it as long as it does not change. The controller at the battery, on contrast, has the goal of discharging the battery to a constant user-defined power P_{ref} (80 W in the experiments shown below), cf. Scenario II in Section 2.2. To do this, the controller must adjust the voltage respectively current so that the desired target power is delivered. The MPPT from the inverter and the control algorithm from the controller must harmonize to the effect that the constant user-defined reference power is maintained as far as possible.

We first describe the controller by itself. It is designed as a buck converter that realizes the hyperbolic *I-V* characteristic $I(V) = P_{\mathrm{ref}}/V$ and thus constant *P-V* characteristics $P(V) = P_{\mathrm{ref}}$, as shown in Fig. 3d.

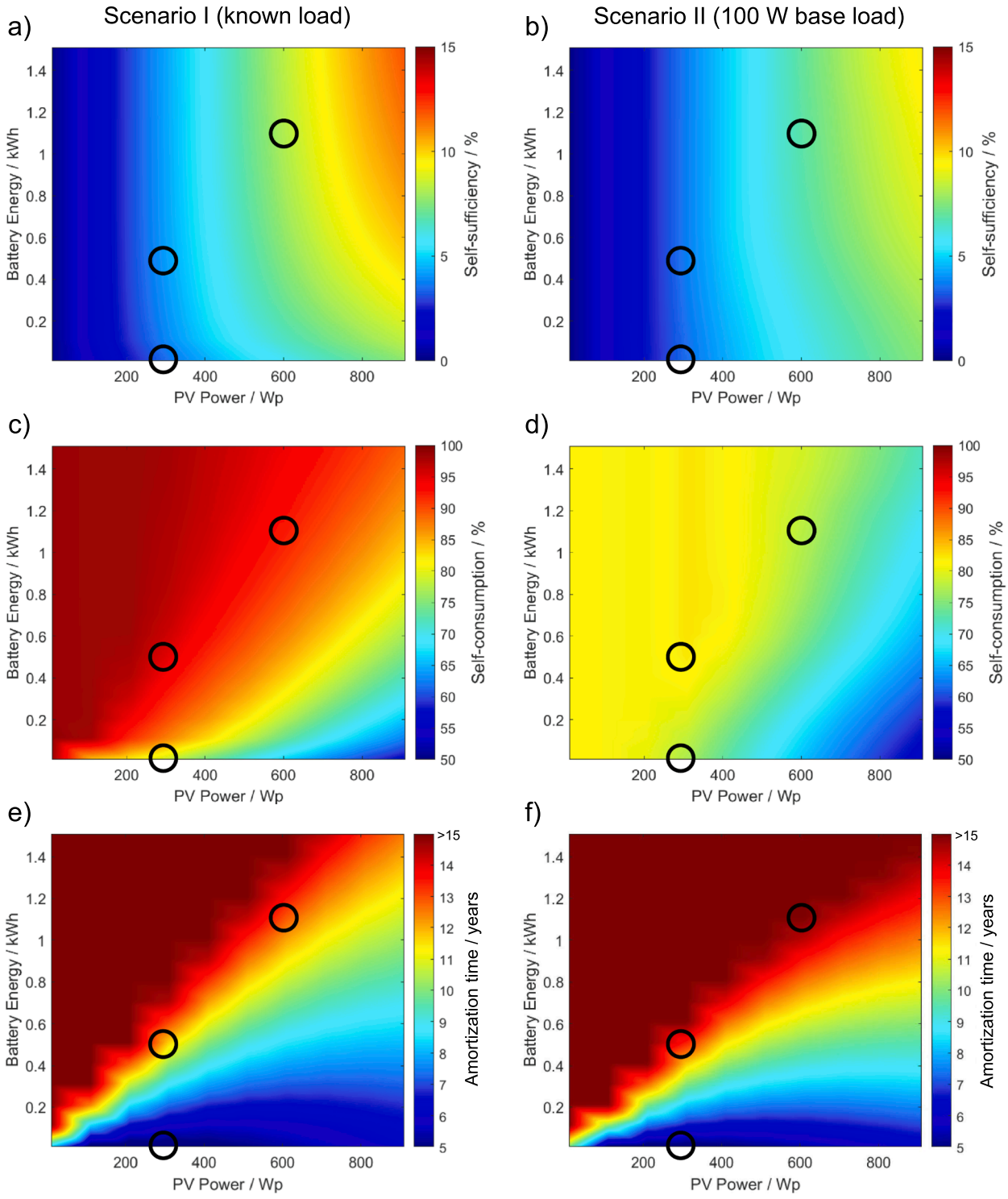

Fig. 5. Results of annual simulations of the micro-PV/battery system: key performance indicators as function of PV peak power and battery energy. The left panels show results for Scenario I (known load), the right panels for scenario II (100 W baseload coverage). a), b) Self-sufficiency (SS, equation (2), c), d) self-consumption (SC, equation (24), e), f) amortization time (AT, equation (23). Simulations were carried out for a PV inclination of 45°. The circles indicate system sizes investigated in the present study experimentally (two bottom left circles) and in more detailed simulations (top right circle).

For this purpose, a control algorithm was implemented, whose flow chart is shown in Fig. 4c, which increases the duty cycle of the buck converter when the measured power is too low and decreases it when the measured power is too high.

Even though these hyperbolic *I-V* characteristics deviates strongly from the typical convex shape of a solar cell characteristics, the experiment shows that this behavior is suitable to ensure the power extraction at the battery with the desired setpoint in interaction with the MPPT of the inverter. One advantage of this control method is that the battery voltage, which also decreases when the SOC value decreases, is automatically compensated for, as the controller then simply draws more current from the battery so that the product of the two values corresponds to the power setpoint.

4. Results and discussion

4.1. Simulation results

Simulations were carried out to show the influence of PV peak power and battery energy on the annual system SC, SS, AS and AT. Fig. 5 shows three of these indicators as contour plots, where the x axis shows the PV peak power and the *y* axis the battery energy. The left and right panels show systems operated in energy management Scenario I (known load) and II (100 W baseload), respectively. In the experimental setup we have used a commercial micro-PV system with 300 Wp power and integrated a LIB with 555 Wh energy. This specific system size is indicated by circles in Fig. 5. Additionally, a system with double values (600 Wp/1110 Wh) is indicated, as well as a reference system without battery (300 Wp/0 Wh).

Panels a) and b) in Fig. 5 show the SS. It increases mainly with increasing PV power. For small PV power $<$ 300 Wp, SS is almost independent of battery energy. This is due to the fact that, for small PV power, most of it can be consumed directly during the day by the household. For PV powers above ca. 600 Wp, SS increases with increasing battery energy. SS is slightly higher in Scenario I (left panels) compared to Scenario II (right panel). The SC is shown in panels c) and d). With increasing PV power, SC strongly decreases, but can be significantly increased by increasing battery energy. The effect is more pronounced in Scenario I compared to Scenario II. The AT is shown in panels e) and f). It is clearly smallest (around 5 years) and therefore the systems are most economically viable without a battery. The only small increase of SS (panels a and b) leads to a strong increase of AT with increasing battery energy. Yet, for large PV power $>$ 600 Wp, a small battery $<$ 400 Wh only moderately increases AT from around five to around seven years. The two Scenarios I and II behave similar.

The main results for the specific setups indicated by circles are summarized in Table 3. The 300 Wp/555 Wh system shows a high SC of 95.7 % in Scenario I, which drops to 82.2 % in Scenario II (100 W base load). The SS is 4.2 % and 3.6 %, respectively. Additionally, the simulation results of both systems including a variation of the PV module installation angle and the base load coverage are listed. The results clearly show that adding battery storage to the micro-PV system significantly increases SS, SC and AS. Comparing Scenario I with Scenario II, it can be seen that the former performs best due to the more elaborated energy management. The results furthermore show that a system with a baseload coverage of 100 W is only slightly different from a system with a baseload coverage according to the VDEW profile. If the results of the different installation angles are compared, it can be seen that, as expected, a 45° installation angle provides better results. Nevertheless, the PV self-consumption is significantly higher in the case of a 90° installation, due to the lower sun in the transition months and in winter.

Exemplary dynamic simulation results for a 600 Wp/1110 Wh system operated in Scenarios I and II are shown in Fig. 6. Panels a) and b) show the dynamic power of all subsystems during two exemplary summer days, c) and d) the battery SOC during these summer days and in e) and f) the SOC over the whole year. From panels a) and b) it can be seen that battery power is the key control variable. The battery is charged ($P_{\mathrm{batt}} < 0$) as soon as PV power exceeds the load and discharged ($P_{\mathrm{batt}} > 0$) when the load exceeds the PV power. If the load can no longer be covered by firstly the PV and secondly the battery, the power is taken from the grid. In panel b) the base load coverage is visible: battery power is 100 W throughout large part of the nights. The SOC is shown in panels c) and d). While the SOC in Scenario I decreases rapidly and reaches zero during the evening due to the high load demand of the household, Scenario II ensures a steady discharge of the battery so that the household can be supplied with self-generated electricity until late at night. This finding is reflected in the annual SOC performance (panels e) and f)). The SOC in Scenario I is generally lower, in particular in the winter and transition months, than that in Scenario II.

Overall, the simulations show that the integration of battery storage into a micro-PV system increases the performance characteristics in terms of SC, SS and AS. However, it strongly increases the cost of the system and therefore its AT.

4.2. Experimental results

After having discussed the theoretical performance of micro-PV/battery systems, this section presents experimental results of the two investigated interconnection architectures. Three-day tests were performed in each case. The respective test results are shown in Fig. 7 for the passive hybrid system and in Fig. 8 for the active hybrid system. Here, the solar irradiation is plotted in panel a), the voltage curves in panel b), the current curves in panel c), the power curves of the main components in panel d), the AC-side power curve in panel e), and the SOC of the battery in panel f). In addition to the two interconnection

Table 3
Simulation results for different component dimensions, energy management strategies, and inclination angles.

	45° inclination			90° inclination		
	Self-sufficiency/%	**Self-consumption/%**	**Annual saving/€**	**Self-sufficiency/%**	**Self-consumption/%**	**Annual saving/€**
	$E_{\mathrm{batt}} = 555$ Wh, $P_{\mathrm{PV}} = 300$ W					
No battery	3.41	77.2	81.4	2.82	83.2	67.4
Scenario I (known load)	4.23	95.7	101	3.34	98.6	79.8
Scenario II (50 W)	3.57	80.9	85.2	2.93	86.6	70.0
Scenario II (100 W)	3.63	82.2	86.7	2.87	84.6	68.5
Scenario II (VDEW profile)	3.61	81.8	86.1	2.95	86.9	70.3
	$E_{\mathrm{batt}} = 1110$ Wh, $P_{\mathrm{PV}} = 600$ W					
No battery	5.79	65.6	138	5.01	73.8	120
Scenario I (known load)	8.16	92.4	195	6.57	96.8	184
Scenario II (50 W)	6.43	72.9	154	5.61	82.9	134
Scenario II (100 W)	6.87	77.9	164	5.80	85.5	138
Scenario II (VDEW profile)	6.89	78.1	165	5.82	85.9	139

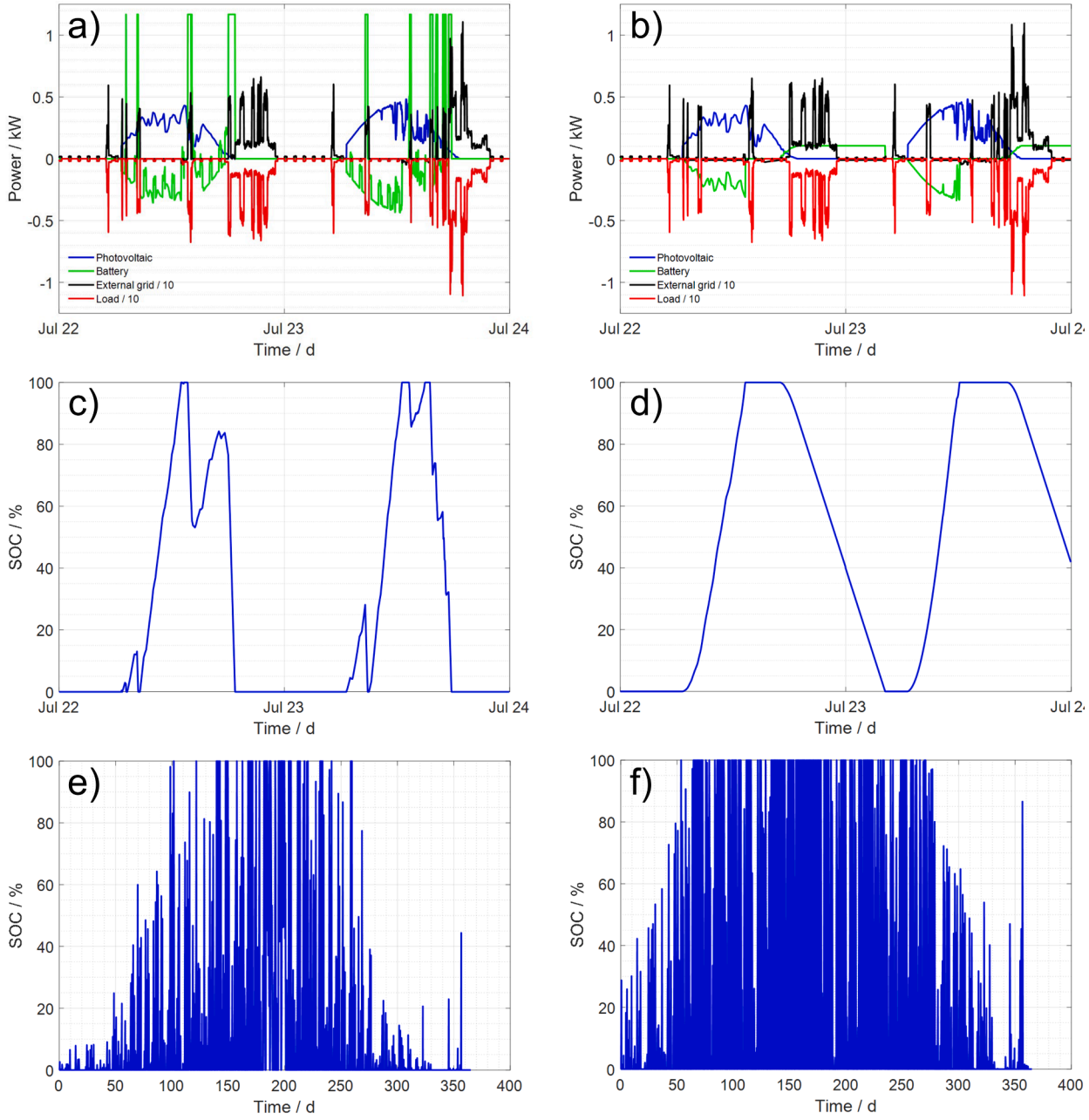

Fig. 6. Simulation results of Scenario I (known load) on the left and Scenario II (100 W base load coverage) on the right for a 600 Wp/1110 Wh micro-PV/battery system. Note that in panels a) and b) the power curves of the household (load) and the external grid were scaled for clarity.

architectures, test results for the reference system without battery are provided for comparison. They are shown in Fig. 9 in the same layout. It should be noted that in the figures, a positive sign indicates the entry of power into the micro-PV system, while a negative sign describes the exit, so that the power balance

$$P_{\mathrm{PV}}(t) + P_{\mathrm{batt}}(t) + P_{\mathrm{R}}(t) + P_{\mathrm{inv,DC}}(t) = 0 \tag{32}$$

is always satisfied, where P_{R} is the thermal power loss over the resistor in case of the passive hybrid system and $P_{\mathrm{inv,DC}}$ is the DC power fed into the inverter.

We start by discussing the behavior of the passive hybrid system (Fig. 7). The solar irradiation (panel a) shows the expected day-night behavior, where the days were rather cloudy. The voltages of the three components (panel b) exhibit a dynamic behavior. Through parallel electrical connection of PV and battery, PV voltage is equal to battery voltage (the slight difference originates from the diode), which in turn depends on SOC: voltage is self-similar to SOC (panel f). The inverter voltage shows an almost constant value through the full experiment (except apparent fast fluctuations): It is buffered from PV and battery by the resistor. The currents (panel c) show the strong interaction between the components. During the first day (approx. first 8 h of data), the battery is charged ($I_{\mathrm{batt}} < 0$) by a part of the PV current ($I_{\mathrm{PV}} > 0$), while another part is delivered to the inverter (for which always $I_{\mathrm{inv}} < 0$). This increases the SOC of the battery and therefore increases the voltage level of the system. As the system voltage increases, the generated current decreases according to the *I-V* characteristics of the PV modules. This self-regulating effect ensures that the battery is not overcharged as the test progresses. During the afternoon, as solar irradiation and PV generation decrease, the current demanded by the inverter's MPP tracker is not only met by the PV, but also by the battery: the battery current shows a sign change. As consequence, SOC

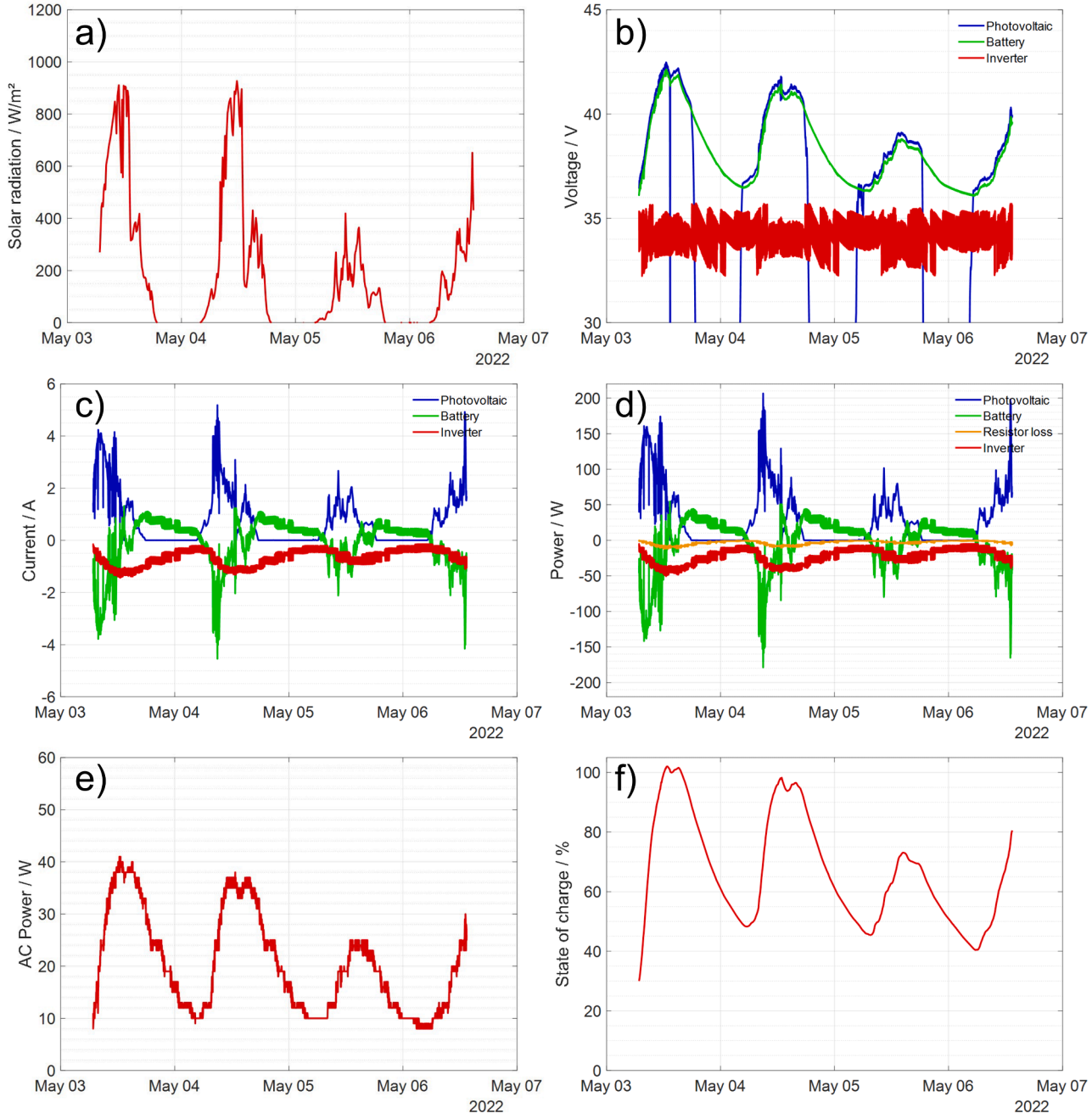

Fig. 7. Passive hybrid system behavior during three-day operation. a) Solar irradiation, b) voltage, c) current, d) DC power, e) AC power, f) and battery SOC. The results demonstrate the successful day-night PV energy shift by integrating a battery into the micro-PV system.

decreases and so does the system voltage. At night, the PV voltage drops to zero (the importance of the diode in preventing the battery from discharging into the PV modules becomes apparent), so does PV current. Now only the battery continues to deliver current to the inverter, with the discharge rate limited by the resistor. The inverter current is never zero and therefore the inverter is in continuous operation throughout the experiment. The behavior of the DC power (panel d) is similar to that of the current. However, an additional variable, the power lost at the resistor in form of heat, is included in the plot. On average, the loss over the resistor is 11.0 % with respect to the total amount of energy that could have been supplied to the inverter. The AC power (panel e) demonstrates continuous inverter operation both during the day and at night, with a fluctuating AC power between 40 W and 10 W. The SOC curve (panel f) shows that the system does not utilize the entire battery capacity: it is never fully discharged during the nights before charging during the day. The depth of discharge during the three-day test was a maximum of 60 %. This could be improved by using a resistor with lower resistance. Overall, the dynamic behavior of all measured variables nicely demonstrates the self-regulating performance of the passive hybrid architecture, which does not rely on any battery control.

During the active hybrid system tests (Fig. 8), the weather was clearer compared to the passive hybrid tests (panel a) – in particular the second day is nearly cloud-less. As the battery is coupled to the system via the controller, the battery voltage (panel b) is independent of the PV and inverter voltages and follows a pattern of discrete charge and discharge cycles. The test starts with an almost full battery (panel f), therefore the battery voltage is essentially constant during the first day. During the night-time, the battery controller is in discharge mode:

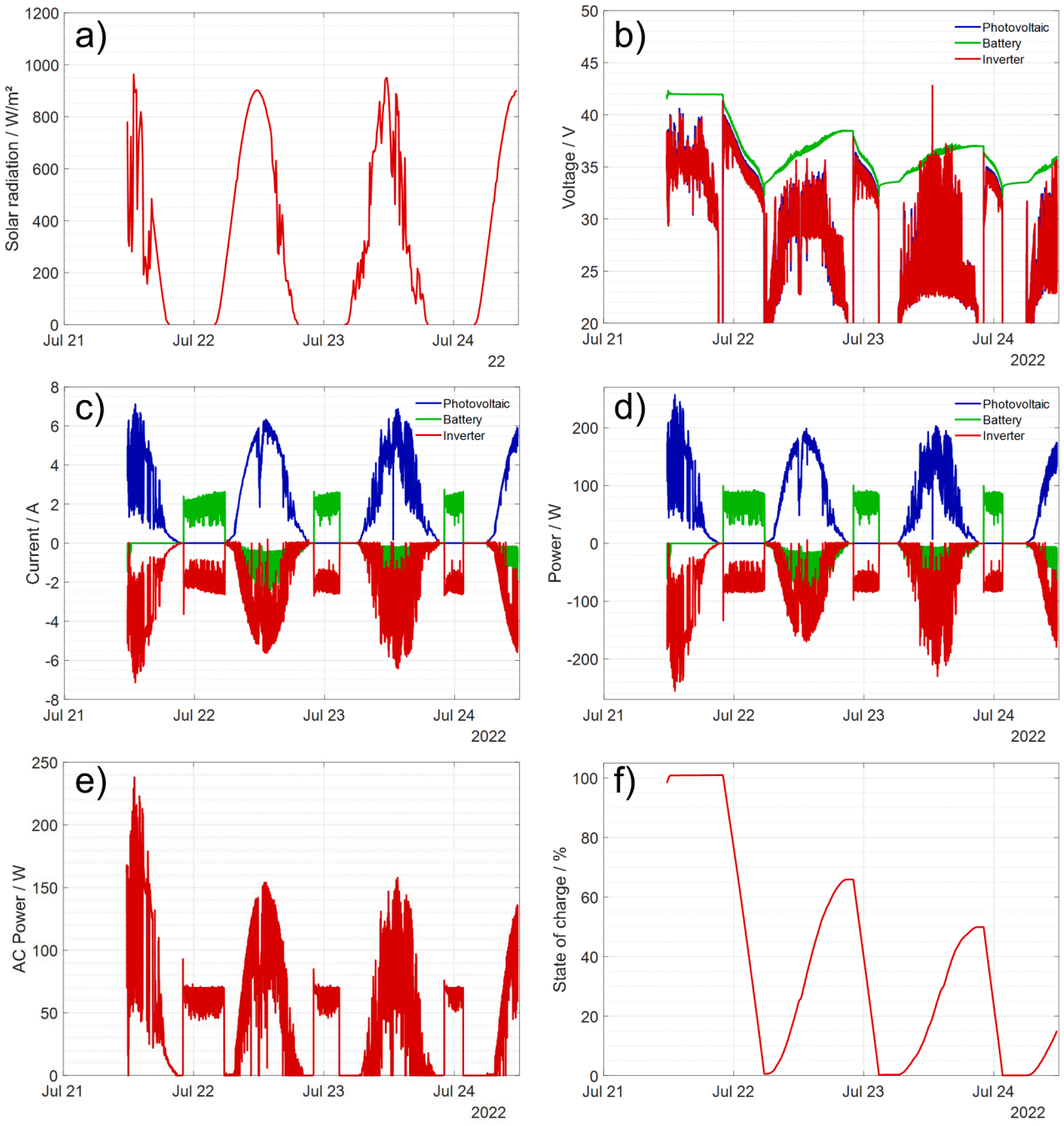

Fig. 8. Active hybrid system behavior during three-day operation. a) Solar irradiation, b) voltage, c) current, d) DC power, e) AC power, f) and battery SOC. The results demonstrate the successful day-night PV energy shift by integrating a battery into the micro-PV system.

battery voltage decreases and inverter voltage roughly follows the battery voltage, but with a voltage drop due to the controller resistance. When the sun rises at the second day, the controller switches to charge mode and the battery voltage steadily increases. During the day, the PV voltage is similar to the inverter voltage since both are connected in parallel (small differences are due to resistances in the system). This voltage is affected by the PV load, resulting from the parallel MPPT operation, and the solar irradiation. The voltage shows strong short-term fluctuation, which probably is a result of the inverter's MPPT. The discrete charge/discharge phases are also observed in the currents (panel d) and powers (panel e). As the battery reaches its full charge on the first day, the controller sleeps so that the battery current and power are zero and the full portion of the PV current flows to the inverter. At 10 p.m., the controller switches to discharge mode and current flows from the battery to the inverter. For this particular experiment, the controller was set to regulate an output power of 80 W: this setpoint is held, albeit with fluctuation, overnight until the battery is empty. As the discharge progresses, the average battery current increases to compensate for the reduced battery voltage while maintaining the power setpoint. The discharge ends when the battery is empty, and the system returns to the idle state so that no battery current flows. Compared to the passive hybrid, the inverter current has zero points, so the inverter is not in continuous operation. Every day at 6 a.m., the charging process starts. Based on the controller settings, we limit the battery current to an approximate maximum of 2.5 A. Therefore, most of the PV current generally flows to the inverter, but fluctuates at times with a higher

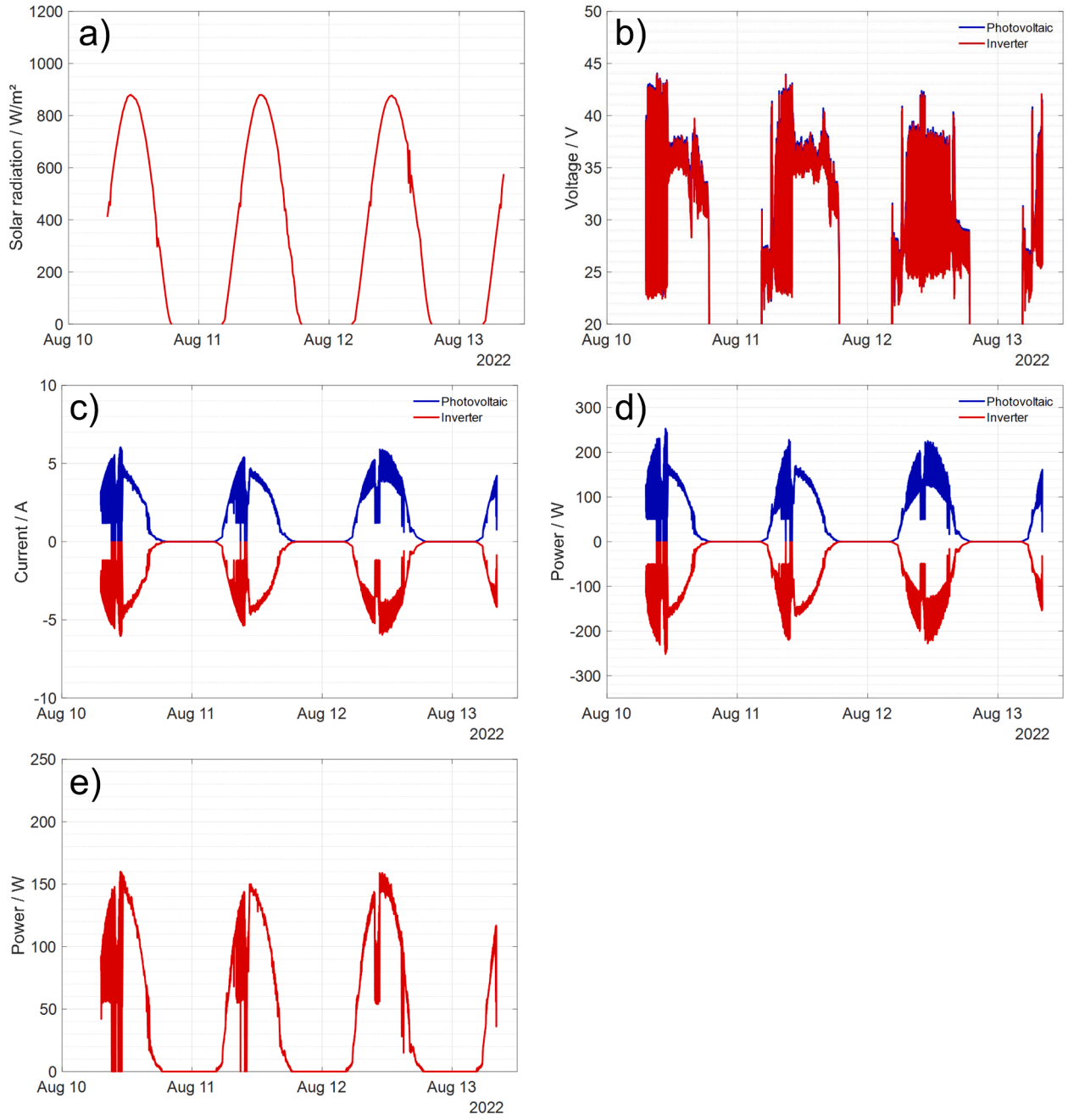

Fig. 9. Reference system behavior during three-day operation. a) Solar irradiation, b) voltage, c) current, d) DC power, e) and AC power. The system does not include a battery and therefore no day-night PV energy shift is possible.

battery current based on the current operating step of the two independent MPPTs (micro-PV inverter and battery controller). Note that the current curve shows a significant local minimum in PV current at about 11 a.m. on each day. This is due to partial shading of the test setup. The AC power (panel e) is discontinuous due to the fixed charge/discharge cycles and the draining of the battery during the nights. On the first day, the AC power is maximum because the battery charge mode is not in operation due to a full battery. Depending on irradiation and system conditions, up to 238 W is delivered. During the nights the output is around 70 W. This is less than the regulated 80 W, which can be attributed to inverter losses (cf. next Section). On the second day, charging and inverter operation take place in parallel. Consequently, less power is available to the inverter during the day, up to 154 W. Since the battery was not fully charged during the day, the duration of battery discharge on the second night is shorter than on the first night. Concerning SOC (panel f), the active hybrid does not use the entire available battery capacity, similarly to the passive hybrid, although for different reasons: The battery is fully drained every night, but not fully recharged during the days. This could be improved by changing the maximum charging current.

The test results for the reference system without battery are shown in Fig. 9. The three days showed almost cloud-free weather (panel a). Due to the simpler setup, the voltage (panel b), current (panel c) and DC power (panel d) curves are much simpler compared to the two hybrid architectures. Obviously, as the reference system lacks a battery, it does not provide any power during the night. The AC power (panel e) clearly shows the effect of partial shading of the PV panels every day at around 11 a.m.

The motivation for integrating a battery into a micro-PV system is the possibility to shift PV energy from the day into the night. With the passive hybrid architecture, the PV energy shift can be clearly seen in the curves of AC power and SOC. Together with the PV energy fed into the household during the day, this results in an overall base load coverage that can be used to supply low continuous loads and household appliances such as refrigerators. Overall, the data demonstrates that the system is capable of maintaining stable operation under real conditions. With the active hybrid architecture, the PV energy shift is also demonstrated and can be clearly seen in both the AC power and the SOC. Although the inverter power is intermittent compared to the passive hybrid, the output power is higher. We believe that with further controller optimization, e.g., changing the discharge rate and timing of the operating modes, the inverter operation can be nearly continuous to achieve uniform baseload coverage.

4.3. Efficiency

For each system, we calculated the system efficiency η_{system} as the ratio between the electric energy $E_{\text{inv,DC}}$ supplied to the inverter at the DC input and the solar irradiation energy E_{irr} received according to

$$\eta_{\text{system}} = \frac{E_{\text{inv,DC}}}{E_{\text{irr}}} = \frac{\int_0^t P_{\text{inv,DC}}(t)\mathrm{d}t - E_{\text{batt}}(t_0) + E_{\text{batt}}(t)}{\int_0^t P_{\text{irr}}(t)\mathrm{d}t} \tag{33}$$

We correct for the energy content of the battery, E_{batt}, before and after the test. In this calculation, the efficiency of the PV modules is included, but the efficiency of the inverter is not considered. Therefore, η_{system} allows the comparison of the different hybridization architectures independent of the load–dependent inverter efficiency. The latter is determined in a separate step. Differences in areal irradiance between the irradiance measurement system and the PV module caused by orientation and inclination are also not considered. The calculation is repeated for each system, once with the total three-day data and once with one-day data based on the day with the highest total solar irradiance out of the three days.

The results are shown in Fig. 10 and summarized in Table 4. The solar irradiation values are lowest for the passive hybridization case (Fig. 10a). This results in the likewise lowest DC energy. For the other two cases, the solar irradiation values are similar. The system efficiencies over the full tests were quantified as 6.95 %, 8.44 %, and 7.99 % for the passive hybrid, active hybrid, and reference systems, respectively (Fig. 10b). The lower efficiency of the passive hybrid results from the heat losses at the series resistor, which amounts to 0.25 kWh (0.85 % of the solar irradiation) over the three-day test. The comparatively highest efficiency of the active hybrid demonstrates the effectiveness of the parallel MPPT operation, and the low losses of the controller compared to those of the components of the passive hybrid system. The numbers demonstrate the feasibility of both hybrid systems. A further quantitative comparison is difficult due to the different irradiation conditions.

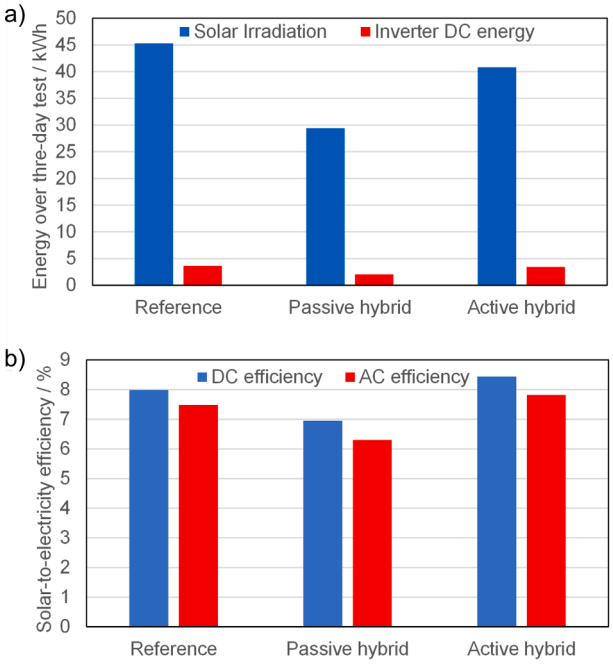

Fig. 10. Comparison of the performance of the three investigated systems over the three-day measurement periods. a) Solar energy input and DC energy output, b) solar-to-electricity DC and AC efficiencies. The values are also given in Tables 4 and 5. AC efficiency was calculated as product of η_{system} and η_{inverter}.

Table 4
Solar-to-DC efficiencies η_{system} (cf. Eq. 33). The DC energy is corrected for the difference in battery charge at beginning and end of experiment.

System	Solar irradiation/ kWh	Inverter DC Energy/ kWh	Efficiency/ %
Reference			
Whole test	45.3	3.62	7.99
Best day	14.8	1.17	7.91
Passive hybrid			
Whole test	29.4	2.04	6.95
Best day	10.5	0.61	5.80
Active hybrid			
Whole test	40.8	3.45	8.44
Best day	15.0	1.30	8.65

The electrical efficiency of the inverter η_{inverter} was calculated by comparing the ratio between the AC energy delivered and the DC energy supplied according to

$$\eta_{\text{inverter}} = \frac{\int_0^t P_{\text{inv,AC}}(t)\mathrm{d}t}{\int_0^t P_{\text{inv,DC}}(t)\mathrm{d}t} \tag{34}$$

Both quantities are shown in Fig. 11 in which the DC input and AC output power of the inverter are plotted over the course of the three-day experiments. The plots are smoothed with a suitable moving average window to increase clarity. Table 5 summarizes the results. Note these values are not corrected for the battery energy, in comparison to Table 4. The three-day efficiencies were quantified as 90.7 %, 92.7 %, and 93.6 % for the passive hybrid, active hybrid, and reference systems, respectively. The reference system clearly has the highest efficiency. This is likely due to the higher average power during inverter operation, resulting in a more favorable inverter operation point. It should be noted that the micro–PV inverter is designed for the use without battery. When the three-day inverter efficiency is combined with the three-day system efficiencies in Table 4, the overall solar-to-AC-efficiencies $\eta_{\text{system}}\cdot\eta_{\text{inverter}}$ are 6.30 %, 7.82 % and 7.48 % for the passive, active and reference systems, respectively (see Fig. 10b).

5. Summary and conclusions

Micro-PV systems have significant potential for increasing renewable energy supply on a decentralized basis. It is accessible to the broad public at low investment costs and does not require professional installation. So far, commercial micro-PV systems, different to larger rooftop PV systems, do not feature the possibility to integrate battery storage. In the present work, we have successfully integrated a commercial lithium-ion battery from an electric bicycle into a commercial micro-PV system, resulting in a 300 Wp/555 Wh PV/battery/inverter system. The particular challenge was that neither of the two individual components (micro-PV system and battery) was to be modified. To this

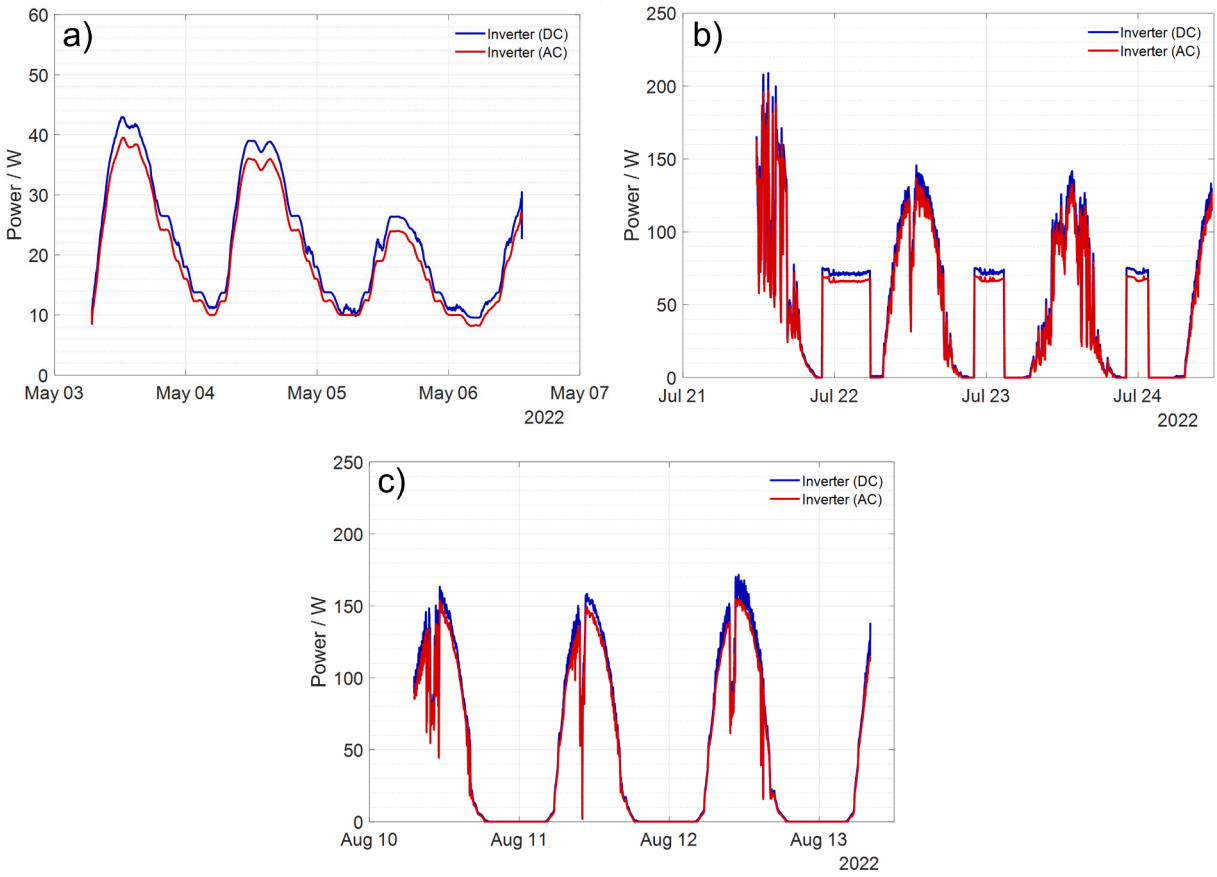

Fig. 11. Comparison of inverter DC and AC power during three-day operation of the a) passive hybrid system, b) active hybrid system, c) and the reference system.

Table 5
DC-to-AC efficiencies $\eta_{inverter}$ (cf. Eq. 34). Different to Table 4, the DC energy input is not corrected for the battery energy.

System	Energy input (DC)/ kWh	Energy output (AC)/ kWh	Efficiency/ %
Reference			
Whole test	3.62	3.39	93.6
Best day	1.17	1.10	93.6
Passive hybrid			
Whole test	1.76	1.60	90.7
Best day	0.61	0.56	91.2
Active hybrid			
Whole test	3.91	3.62	92.7
Best day	1.51	1.40	92.8

goal, two different system architectures, termed here active and passive hybrid architecture, were developed, realized, and tested in continuous operation under real conditions. The passive hybrid architecture used a parallel electrical connection between PV and battery without intermediate voltage conversion. In order to avoid excessive current when the battery is subjected to the inverter's MPP tracker, an additional resistor was added to the system. The active hybrid architecture is based on a controlled DC-DC converter based on a bidirectional buck/boost converter. Appropriate control strategies for battery charge (during day) and discharge (during night) were implemented. To compare the two new systems in terms of performance and efficiency, a reference system without battery was also investigated.

Both micro-PV/battery systems were shown to provide continuous and stable operation over three days under real conditions and shift PV energy from day into at night. Thus, the feasibility of both connection architectures was demonstrated. The passive hybrid system is conceptionally simple and allows continuous inverter operation advantageous to provide household base-load coverage. However, in the tests it showed the lowest efficiencies. The active system shows intermittent inverter operation but has higher system efficiencies. It should be emphasized that neither architecture requires a change of the commercial micro-PV system components or the commercial lithium-ion battery. Therefore, a retrofitting of existing micro-PV systems is possible.

The study was supported by simulations of micro-PV/battery systems in a single-family house operated over one year. The simulations showed that integration of a battery into a micro-PV system allows to increase self-sufficiency, self-consumption and annual savings. However, for the component sizes used in the present experiments, the improvement was only moderate (self-sufficiency increased from 3.41 % for a system without battery to 3.63 % for a system operating in baseload scenario). The advantage of including a battery increases with increasing PV power. However, the battery cost is significant.

The present study has several limitations. Firstly, the three investigated systems (passive hybrid, active hybrid, reference without battery) were operated over durations of only three days. The solar irradiation conditions were different for the three tests. The observed performance and efficiencies are therefore only qualitatively comparable. In future studies, three systems should be operated simultaneously and over extended periods of time, possibly during different seasons. Secondly, neither of the developed systems provides functionality to avoid battery overcharge or overdischarge – they completely rely on the battery's own management system. For safety reasons, battery monitoring should be included in the hybrid system. Finally, only one single lithium-ion

battery was tested. However, there is a large number of different electric bicycle battery sizes and manufacturers. For a broad applicability, the system setup should be adapted for more flexibility, which will probably need to include communication with the battery. These limitations provide ample room for future studies.

Declaration of Competing Interest

The authors declare that they have no known competing financial interests or personal relationships that could have appeared to influence the work reported in this paper.

Acknowledgements

This work was funded by the badenova AG & Co. KG, Freiburg, Germany, as part of the Innovation Fonds Climate and Water Protection, Project No. 2020-08. The authors thank Peter Majer (badenova) for detailed discussions and support of this work, as well as Amanda Tofic (Hochschule Offenburg) for supporting the passive hybridization experiments. WB would like to acknowledge funding from the Land Baden-Württemberg and the European Union within the framework of the BaBa-PV project (FEIH_ProT_2518605).

References

[1] Kebede, A.A., Kalogiannis, T., Van Mierlo, J., Berecibar, M., 2022. A comprehensive review of stationary energy storage devices for large scale renewable energy sources grid integration. Renew. Sustain. Energy Rev. 159, 112213.
[2] Rana, M.M., Uddin, M., Sarkar, M.R., Shafiullah, G.M., Mo, H., Atef, M., 2022. A review on hybrid photovoltaic – Battery energy storage system: Current status, challenges, and future directions. J. Storage Mater. 51, 104597.
[3] Figgener, J., Stenzel, P., Kairies, K.-P., Linßen, J., Haberschusz, D., Wessels, O., Angenendt, G., Robinius, M., Stolten, D., Sauer, D.U., 2020. The development of stationary battery storage systems in Germany – A market review. J. Storage Mater. 29, 101153.
[4] Haas, R., Kemfert, C., Auer, H., Ajanovic, A., Sayer, M., Hiesl, A., 2022. On the economics of storage for electricity: current state and future market design prospects. WIREs Energy Environ. 11, e431.
[5] Volker Quaschning, 2015. *Regenerative Energiesysteme*, 9th edition. Carl-Hanser-Verlag.
[6] Joos, S., Weißhar, B., Bessler, W.G., 2017. Passive hybridization of a photovoltaic module with lithium-ion battery cells. A model-based analysis. J. Power Sources 348, 201–211.
[7] Leible, V., Bessler, W.G., 2021. Passive hybridization of photovoltaic cells with a lithium-ion battery cell: an experimental proof of concept. J. Power Sources 482, 229050.
[8] Belhachat, F., Larbes, C., 2018. A review of global maximum power point tracking techniques of photovoltaic system under partial shading conditions. Renew. Sustain. Energy Rev. 92, 513–553.
[9] Yang, S., Chen, W., Kim, H., 2021. Building energy commons: Three mini-PV installation cases in apartment complexes in Seoul. Energies 14, 249.
[10] Astakhov, O., Merdzhanova, T., Kin, L.-C., Rau, U., 2020. From room to roof: How feasible is direct coupling of solar-battery power unit under variable irradiance? Sol. Energy 206, 732–740.
[11] Unites States Time Corporation, Waterbury, USA, Photoelectric conversion system, Great Britain Patent GB1123035A (7 August 1968).
[12] G. W. Mellors, R. A. Powers, and W. Sheffield, Charging circuit for battery-operated devices powered by solar cells, United States Patent US3921049 (18 November 1975).
[13] Kakimoto, N., Asano, R., 2017. Linear operation of photovoltaic array with directly connected lithium-ion batteries. IEEE Trans. Sustain. Energy 8, 1647–1657.
[14] Paul Ayeng'o, S., Axelsen, H., Haberschusz, D., Sauer, D.U., 2019. A model for direct-coupled PV systems with batteries depending on solar radiation, temperature and number of serial connected PV cells. Sol. Energy 183, 120–131.
[15] Agbo, S.N., Merdzhanova, T., Yu, S., Tempel, H., Kungl, H., Eichel, R.-A., Rau, U., Astakhov, O., 2016. Development towards cell-to-cell monolithic integration of a thin-film solar cell and lithium-ion accumulator. J. Power Sources 327, 340–344.
[16] Kin, L.-C., Astakhov, O., Lee, M., Haas, S., Ding, K., Merdzhanova, T., Rau, U., 2022. Batteries to keep solar-driven water splitting running at night: performance of a directly coupled system. Solar RRL 6, 2100916.
[17] Chibuko, U., Merdzhanova, T., Weigand, D., Ezema, F., Agbo, S., Rau, U., Astakhov, O., 2023. Module-level direct coupling in PV-battery power unit under realistic irradiance and load. Sol. Energy 249, 233–241.
[18] Gibson, T.L., Kelly, N.A., 2010. Solar photovoltaic charging of lithium-ion batteries. J. Power Sources 195 (12), 3928–3932.
[19] Shcherbachenko, S., Astakhov, O., Chime, U., Kin, L.-C., Ding, K., Pieters, B., Rau, U., Figgemeier, E., Merdzhanova, T., 2023. Efficient power coupling in directly connected photovoltaic-battery module. Solar RRL 7 (3), 2200857.
[20] Vega-Garita, V., Ramirez-Elizondo, L., Narayan, N., Bauer, P., 2019. Integrating a photovoltaic storage system in one device: a critical review. Prog. Photovolt Res. Appl. 27, 346–370.
[21] Hoppmann, J., Volland, J., Schmidt, T.S., Hoffmann, V.H., 2014. The economic viability of battery storage for residential solar photovoltaic systems – A review and a simulation model. Renew. Sustain. Energy Rev. 39, 1101–1118.
[22] Roberts, J.J., Mendiburu Zevallos, A.A., Cassula, A.M., 2017. Assessment of photovoltaic performance models for system simulation. Renew. Sustain. Energy Rev. 72, 1104–1123.
[23] Seane, T.B., Samikannu, R., Bader, T., 2022. A review of modeling and simulation tools for microgrids based on solar photovoltaics. Front. Energy Res. 10.
[24] Milosavljević, D.D., Kevkić, T.S., Jovanović, S.J., 2022. Review and validation of photovoltaic solar simulation tools/software based on case study. Open Phys. 20, 431–451.
[25] Weißhar, B., Bessler, W.G., 2017. Model-based lifetime prediction of an LFP/graphite lithium-ion battery in a stationary photovoltaic battery system. J. Storage Mater. 14, 179–191.
[26] K. Böhler, M. Wülker, and R. Behmann, "Weather data of Offenburg University of Applied Sciences". https://wetterstation.hs-offenburg.de/ (2008-2022).
[27] Klucher, T.M., 1979. Evaluation of models to predict insolation on tilted surfaces. Sol. Energy 23 (2), 111–114.
[28] SMA Solar Technology AG, "Sunny Island 5048U, Datasheet," (2014).
[29] N. Pflugradt and B. Platzer, "Verhaltensbasierter Lastprofilgenerator für Strom- und Warmwasser-Profile," Proceedings of the 22. Symposium Thermische Solarenergie, Bad Staffelstein, Germany (2012).
[30] R. Bitterer and B. Schieferdecker, "Repräsentative VDEW-Lastprofile. VDEW Materialien, M-32/99," Frankfurt am Main (1999).
[31] Bundesnetzagentur and Bundeskartellamt, *Monitoringbericht 2022*, 2022.
[32] Bosch Solar Energy AG, "Bosch Solar Module c-Si M60 EU30014 Typ M235 3BB, Datasheet," (2012).
[33] Birkl, C.R., Roberts, M.R., McTurk, E., Bruce, P.G., Howey, D.A., 2017. Degradation diagnostics for lithium ion cells. J. Power Sources 341, 373–386.
[34] Feng, X., Ouyang, M., Liu, X., Lu, L., Xia, Y., He, X., 2018. Thermal runaway mechanism of lithium ion battery for electric vehicles. A review. Energy Storage Mater. 10, 246–267.
[35] Kupper, C., Spitznagel, S., Döring, H., Danzer, M.A., Gutiérrez, C., Kvasha, A., Bessler, W.G., 2019. Combined modeling and experimental study of the high-temperature behavior of a lithium-ion cell: differential scanning calorimetry, accelerating rate calorimetry and external short circuit. Electrochim. Acta 306, 209–219.
[36] Hohm, D.P., Ropp, M.E., 2003. Comparative study of maximum power point tracking algorithms. Prog. Photovolt: Res. Appl. 11, 47–62.